A recipe for simulating the interannual variability of the Asian Summer Monsoon and its relation with ENSO

by

Annalisa Bracco, Fred Kucharski, Franco Molteni

The Abdus Salam International Centre for Theoretical Physics,
Trieste, Italy

Wilco Hazeleger and Camiel Severijns

Royal Netherlands Meteorological Institute,
De Bilt, NL

Accepted manuscript for publication in Climate Dynamics

Corresponding author address:

Annalisa Bracco
Woods Hole Oceanographic Institution, Po Dept. MS 21
Woods Hole, MA 02543, USA

e-mail: abracco@whoi.edu

Abstract

This study investigates how accurately the interannual variability over the Indian Ocean basin and the relationship between the Indian summer monsoon and the El Niño Southern Oscillation (ENSO) can be simulated by different modelling strategies. With a hierarchy of models, from an atmospherical general circulation model (AGCM) forced by observed SST, to a coupled model with the ocean component limited to the tropical Pacific and Indian Oceans, the role of heat fluxes and of interactive coupling is analyzed. Whenever sea surface temperature anomalies in the Indian basin are created by the coupled model, the inverse relationship between the ENSO index and the Indian summer monsoon rainfall is recovered, and it is preserved if the atmospherical model is forced by the SSTs created by the coupled model. If the ocean model domain is limited to the Indian Ocean, changes in the Walker circulation over the Pacific during El-Niño years induce a decrease of rainfall over the Indian subcontinent. However the observed correlation between the ENSO and the Indian Ocean Zonal Mode (IOZM) is not properly modelled and the two indices are not significantly correlated, independently on season. Whenever the ocean domain extends to the Pacific, and ENSO can impact both the atmospheric circulation and the ocean subsurface in the equatorial Eastern Indian Ocean, modelled precipitation patterns associated both to ENSO and to the IOZM closely resemble the observations.

1 Introduction

The ocean-atmosphere interannual variability over the Indian Ocean (IO) basin received considerable attention in the last decades (see Schott and McCreary, 2001, Annamalai and Murtugudde, 2004, and Yamagata et al., 2004, for reviews on current knowledge and a summary of open questions).

Between the factors contributing to the IO interannual variability, the El Niño Southern Oscillation (ENSO) is a key player. Its signature in the IO sea surface temperatures (SSTs) consists of a basin scale warming in its positive El Niño phase and general cooling during La Niña conditions, predominantly during the spring season (Tourre and White, 1995; Venzke et al., 2000). El Niño related wind anomalies over the Indian basin are associated to a shift of the Walker circulation, with the preferred location for deep convection moving from the west Pacific warm pool to the central Pacific. Such a shift induces subsidence and reduced precipitation over Indonesia and off Sumatra, and it is generally associated with a below-normal rainfall over India (Rasmusson and Carpenter, 1983; Shukla and Paolino, 1983; Reverdin et al., 1986; Webster and Yuang, 1992; Hastenrath et al., 1993; Murtugudde and Busalacchi, 1999, among others). Numerous studies have investigated, through the analysis of observational data and model outputs, the physical processes at the base of the relationship between the Indian summer monsoon rainfall (ISMR) and ENSO, and the difficulties associated to the modelling of the observed signal (Shukla, 1987; Ropelewski and Halpert, 1987; Ju and Slingo, 1995; Latif and Barnett, 1995; Lau and Nath, 2000; Wang et al., 2003; Wu and Kirtman, 2004; Lau and Nath, 2004, among others). The extent of the Himalayan/Eurasian snow cover, which affects the strength of land-sea thermal gradient during spring and summer, has also long been considered as a modulator of monsoon anomalies (e.g. Douville and Royer 1996; Webster et al., 1998; Ferranti and Molteni, 1999; Bamzai and Marx 2000). Finally, the variability of SSTs in the Indian Ocean plays a very important role (Shukla, 1975; Hackert and Hastenrath, 1986; Arpe et al., 1998; Slingo and Annamalai, 2000; Lau and Nath, 2000; Li and Zhang, 2002; Molteni et al., 2003).

Recently, focus has been given to the Indian Ocean Zonal Mode (IOZM) (Saji

et al., 1999; Webster et al., 1999), a coupled ocean-atmosphere mode of variability considered by many as internal to the Indian Ocean dynamics. The existence of the IOZM, and more so its independency on ENSO has been (and still is) a matter of intense debate (Iizuka et al., 2000; Rao et al., 2000; Allan et al., 2001; Susanto et al., 2001; Baquero-Bernal et al., 2002; Hastenrath, 2002; Saji and Yamagata, 2003; Krishnamurthy and Kirtman, 2003; Annamalai et al., 2003; Gualdi et al., 2003; Yamagata et al., 2003; Bracco et al., 2005, Fisher et al., 2005). In its positive phase, the IOZM is characterized by colder than average SSTs in the south-eastern tropical Indian Ocean, with anomalously strong upwelling off the coast of Java and Sumatra starting in late spring, and warmer anomalies in the central and western Tropical IO during summer and fall. A common consensus on the influence exerted by the IOZM into the ISMR has not been established so far. It has been shown that positive IOZM events, once triggered, can modulate the precipitation along the northern part of India and the Bay of Bengal in boreal summer by intensifying the local meridional circulation. Low-level wind anomalies can develop as a Rossby wave response suppressing precipitation over the eastern Indian Ocean and enhancing the local monsoon circulation (Slingo and Annamalai, 2000; Annamalai and Liu, 2005). Observation and modelling studies have suggested that the IOZM influence extends to the rainfall over all East Asia, including Japan, (Yamagata et al., 2004) and to the short rain in east Africa in fall (Black et al., 2003; Clark et al., 2003).

In this work we investigate numerically the response of the South Asia summer monsoon to SST variability, focusing on the low-level wind and rainfall signal associated with ENSO and with the IOZM. Our goals are

- to improve our understanding of the physical mechanisms regulating the ISMR;
- to find an experimental set-up able to represent at best the interannual variability over the Indian ocean basin.

To do so, we analyze model outputs from a series of ensemble integrations of increasing complexity, from simulations performed using an atmospheric general

circulation model (AGCM) forced by observed SSTs, to a coupled general circulation model (CGCM) of the Tropical Pacific and Indian Ocean. The multiplicity of integrations in each ensemble improves the statistical significance of our results and allows for evaluating the impact of atmospheric internal variability.

Most AGCMs used in the climate community are incapable of reproducing the observed patterns associated to the ENSO-monsoon relationship whenever forced by prescribed SST anomalies (Sperber and Palmer, 1996). Lau and Nath (2000) pointed out that forced AGCMs may not be able to capture the air-sea coupling in the region. According to their analysis, part of the SST anomalies may arise from atmospheric forcing via surface heat fluxes. In the tropics, and especially over the Indian Ocean, the atmosphere and the ocean surface are intrinsically coupled and it is difficult to establish (and impose) the dominant forcing component. Wu and Kirtman (2004) recently investigated this issue and found the coupling to be essential to recover the observed out-of-phase relationship between ENSO and the ISMR. Similar results have been reported by Wang et al. (2005).

We will show that our model is capable of reproducing the observed signal whenever SST anomalies are generated by an interactive ocean, i.e. both in the coupled integrations and in the case of the AGCM forced by the modeled SSTs anomalies. We also find that whenever the ocean model domain is limited to the Indian Ocean only, the variability associated to the IOZM is uncoupled from ENSO. In this case, the observed ENSO-monsoon relationship can be fully recovered only if the correlation between the two modes in the observations is externally imposed. On the other hand, when the ocean model domain extends to the Tropical Pacific ocean, ENSO and the IOZM appear to be correlated as in the observations (Bracco et al., 2005). That is, the oceanic bridge between the Indian and Pacific Oceans causes the phasing between the IOZM and ENSO to be as in the observations.

In section 2, we describe the model, the ensembles performed in this study and their climatology. The variability in the tropical Indo-Pacific basin for progressively increasing the level of model complexity is analyzed in Section 3. Discussions and conclusions follow in section 4.

2 Model, Configurations and Climatology

The ICTP AGCM used in this work is described in details in Molteni (2003). It is based on a hydrostatic spectral dynamical core (see Held and Suarez, 1994), in the vorticity-divergence form described by Bourke (1974). The parameterized processes include short- and long-wave radiation, large-scale condensation, convection, surface fluxes of momentum, heat and moisture, and vertical diffusion. Convection is represented by a mass-flux scheme that is activated where conditional instability is present, and boundary layer fluxes are obtained by stability-dependent bulk formulae. In this study the AGCM is configured with 8 vertical (sigma) levels and with a spectral truncation at total wavenumber 30. Furthermore, land and ice temperature anomalies are determined by a simple one-layer thermodynamic model. Results of multi-decadal simulations performed with the current 8-level and a previous 7-level version of the model are discussed in Kucharski et al. (2006) and Bracco et al. (2004), respectively.

Monthly varying SST from the HadISST dataset (Rayner et al. 2003) are used to force the AGCM-only integrations for the period 1950-1999. We shall present diagnostics from a series of ensembles generated by using different initial conditions. Each set of initial conditions has been derived by applying random perturbations in the first few time steps, followed by a spin-up integration of one year for the AGCM runs and of 20 years for the coupled simulations.

The ocean model adopted for the coupled experiments is MICOM (the Miami Isopycnic Coordinate Ocean Model) version 2.9 (Bleck et al. 1992), in a regional configuration with 20 vertical levels and 1^oX1^o resolution in the horizontal. MICOM is initialized with climatological winter values from Levitus (Levitus et al. 1994). Further details on the coupling strategy can be found in Hazeleger et al. (2003).

2.1 Experimental set-up

Motivated by the observational evidence and by previous studies, we performed 6 ensemble experiments with either the uncoupled AGCM or the (regionally) coupled model to investigate the connection between the South Asian summer

monsoon rainfall, the IOZM and ENSO, and the model requirements to properly simulate it. Table 1 summarizes the numerical experiments performed, the size of the ensembles and their characteristics.

In ENS3 the ocean model (MICOM) is confined to the tropical Indian Ocean from 32S to 30N and from the coast of Africa to 140E. A 3^o-wide zone south of 32S and east of 140E is used to blend ocean model SSTs to observed values and subsurface quantities to Levitus monthly climatology. The model domain extends into the Pacific Ocean to insure that the dynamics in the Indian basin is the least affected by the blending boundary conditions. We verified the independence of our results on the inclusion of the Western Pacific portion with a three-member ensemble in which the ocean model domain is limited to 110E. By definition, all members are forced by the same SSTs in the Tropical Pacific for the period 1930-1999 outside the OGCM domain. The first twenty years are discarded in the analysis and only the 1950-1999 period is considered.

To confirm and extend the conclusions deduced from the above integrations, in section 4 we consider three runs, each 150 years long, with prescribed climatological SSTs except in the Tropical Indian and Pacific Ocean (32S-30N), where MICOM is coupled to the ICTP AGCM (ENS5). Also in this case a 3^o-wide zone blend the ocean model to climatology. In these integrations, we impose a correction on the SST field forcing the atmosphere (SST_A) with the form

$$SST_A = SST_{cl} + \alpha[SST_O - < SST_O >], \tag{1}$$

where α grows linearly from 0 to 1 during a 20 year spin-up period. [1] Here, SST_{cl} represent the observed monthly climatology, SST_O the ocean model SSTs, and $< SST_O >$ the ocean model monthly climatology. While the AGCM uses heat, moisture and momentum fluxes computed from the corrected SST, fluxes passed to the ocean model are computed with respect to the uncorrected SST field simulated by MICOM. By preventing the occurrence of positive feedbacks amplifying the climate drift of the coupled system, such a correction reduces significantly the SST bias in the equatorial Pacific which occurs in the uncorrected version of model in the same configuration, and allows the simulation a realistic

[1] In our analysis we discarded the spin-up period and the first 30 years of integration.

ENSO cycle. Again, SSTs from ENS5 are used to force the ICTP AGCM in the last ensemble (ENS6). [2]

The SST ocean model error in the south Asian monsoon season (from June to September, JJAS), defined as $< SST_O > - SST_{cl}$, is shown in Fig. 1 for the ENS3 and ENS5 ensembles. In Fig. 2 the model annual-mean vertical section of temperature in the Indian basin at the Equator is presented for the coupled ensembles. In both configurations the model is able to properly represent the observed tilting of the ocean thermocline in the Indian basin. The overall structure of the equatorial thermocline is realistic: In ENS3 is in good agreement with Simple Ocean Data Assimilation products (Carton et al., 2000), while in ENS5 is shallower than observed particularly in the Eastern tropical Indian Ocean.

2.2 The climatology over the Indian Ocean

Before investigating the interannual variability in the various ensembles, it is useful to describe how different configurations are able to reproduce the main features of the climatology during the Indian monsoon summer season, from June to September (JJAS). We focus on the patterns of 925hPa winds and precipitation, shown in Fig. 3. [3] The top-left panels show the observed precipitation climatology from the CMAP (Climate Prediction Center Merged Analysis Precipitation; Xie and Arkin, 1997) dataset. CMAP data, derived from satellite observations, are considered more reliable than reanalysis estimates, but are available only from 1979. Here we use the period 1979-2002; no significant changes are found when only the first 20 years are considered. On the top right, the wind climatology from NCEP reanalysis (Kalnay et al., 1996) at 925hPa is calculated for the 1950-1999 period in boreal summer.

Fig. 3 also shows the climatology for the AGCM forced by observed SSTs (ENS1, panels c-d), for the AGCM with a mixed-layer model in the Indian Ocean (ENS2, panels e-f), for the coupled circulation model, with MICOM integrated in the IO basin (ENS3, panels g-h) and for the AGCM forced in the IO by the

[2] The comparisons between ENS3 and ENS4, and between ENS5 and ENS6 allow us to draw the same conclusions. In the following we will concentrate on ENS4, without repeating figures and discussion for ENS6.

[3] The AGCM performance is comparable at different levels in the lower troposphere, and the analysis of 850hPa winds provides analogous results.

SSTs of the coupled runs (ENS4, panels i-j). The overall features of the observed climatology are reproduced by all ensembles, but significant differences emerge between the various runs. ENS1 tends to underestimate the strength of the monsoon winds, producing a weaker than observed Somali jet and weak westerlies from the ocean into the Indian subcontinent. The AGCM overestimates precipitation over the warm SSTs of the equatorial ocean, while the Indian peninsula is dryer than observed. Over the Bay of Bengal, one rainfall maximum occurs to the south of the observed signal, while another stronger peak is located over Bangladesh and on the foothills of the Tibetan Plateau (whose topography is poorly resolved in the model due to the coarse horizontal resolution). The use of a mixed layer ocean (ENS2) does not change substantially the modelled climatology.

In ENS3, on the other hand, the winds associated with the monsoon circulation are stronger, and carry moisture into the regions of the Indian subcontinent and in the Bay of Bengal. A weak rain maximum upstream of the Western Ghats is also simulated. Less rain falls over the ocean, and the overall precipitation pattern is in better agreement with the observed one. The meridional winds in the vicinity of the Philippine Islands improve and bear a close resemblance to reanalysis.

The summer climatology for ENS4 is very close to that of ENS3, with analogous precipitation patterns, only slightly stronger in intensity.

Changes between ENS1-2 and ENS3-4 are likely to be related to differences in the SST climatology, despite the error of the coupled model in the IO is small and limited to a cooling close to the African coast during JJAS (Fig 1a). Such a cooling is associated to stronger meridional winds off Somalia and to a shallower than observed thermocline in proximity of the African coast, with the consequent upwelling of cooler than observed waters at the surface.

Whenever the fall season (from October to December) is considered (not shown) ENS2 and ENS4 display patterns almost identical to ENS1 and ENS3 respectively. Again AGCM-only runs underestimate the strength of the westerlies winds that bring moisture from the ocean into the Asian land regions. ENS3 and

ENS4 overestimate the total amount of precipitation, but display a more realistic pattern for both winds and rain. In the coupled runs the SST climatology in OND is in better agreement with the HadISST data.

The comparison between observed and modelled climatology has been extended to other quantities, such as velocity potential and winds at different levels. Overall all diagnostics show that, in our model, the introduction of a thermodynamic mixed-layer ocean in the IO basin does not alter the climatology of the ENS1 ensemble, forced by HadISST fields. On the other hand, if the AGCM is forced by the SSTs produced by the dynamical coupled model (ENS4), patterns found in the coupled runs (ENS3) are very well preserved during all seasons. Differences are limited to the intensity of the signal, usually slightly stronger over the ocean in ENS4 compared to the ENS3 case, where the interactive ocean damps part of the internal variability of the atmospheric system.

In ENS5 the AGCM is coupled to MICOM over the tropical Indo-Pacific as described in the previous section and forced by climatological SSTs outside the ocean model domain, while in ENS6 the AGCM is forced by the SSTs of ENS5. The resulting climatology in both ENS5 and ENS6 for winds and precipitation (not shown) is similar to the one of ENS1, with stronger than observed rainfall over the ocean, south of the Indian peninsula. We will show later in the paper that the variability associated with ENSO, on the other hand, differs significantly in ENS5/ENS6 compared to ENS1.

3 The interannual variability

3.1 In the observations

The interannual variability in the Indian Ocean SSTs is relatively weak, when compared to the one of the Pacific, dominated by the ENSO signal (see for example McPhaden, 1999), and is influenced by several factor, as discussed briefly in the introduction. In the following, we will concentrate on the variability associated with ENSO and the IOZM in the Indian monsoon season. Anomalies of various fields associated with different SST indices will be diagnosed by computing regression maps of field anomalies onto such indices, scaled in such a way to

represent anomalies corresponding to one standard deviation of the selected SST index.

The left panels in Fig. 4 show the regression maps onto the Niño-3.4 index (SSTA averaged over the Pacific Ocean region 170^o-120^oW, 5^oS-5^oN) for the HadISST data set (4a) and the NCEP precipitation and 925hPa winds data (4c) over the Indian basin, computed over the period 1950-1999 in JJAS. At the bottom (4e) the regressions are calculated using CMAP precipitation data for the period 1979-2002 and NCEP winds for the same time interval. The SSTA patterns display a warming in the west of the Indian basin, stronger in the Arabian sea, and a cooling in the Indonesian Throughflow region and off Java, extending north in the IO towards Sumatra.

There are significant differences between the NCEP and CMAP precipitation patters. In the NCEP dataset an increase of precipitation characterizes the subtropical West Pacific in the monsoon season. Such a pattern is almost absent in the CMAP dataset. NCEP, on the other hand, shows a decrease of rainfall over the Indian subcontinent in association with El Niño events, in better agreement with the gridded monthly precipitation data from New et al. (1999), obtained from land stations and analyzed by Mason and Goddard (2001) for the period 1951-1952/1995-1996. CMAP data, based on both ground records and satellite measurements, are probably more reliable, but limited to the post-1976 period. It has been shown that the inverse 'traditional' relationship between ENSO and the Indian summer monsoon, i.e. below normal monsoon rainfall associated to El Niño events, underwent a weakening in the post-1976 period (Krishna-Kumar et al., 1999; Kinter et al., 2002; Annamalai and Liu, 2005). In JJAS CMAP displays a larger decrease of rainfall over Indonesia, Java, Sumatra, Malaysia and the West Pacific, in agreement with land station data (Mason and Goddard, 2001).

An index, defined as the difference of area-averaged SST monthly anomalies (SSTAs) in the western tropical IO (WTIO) (50^o-70^oE, 10^oS-10^oN) and in the south-eastern tropical IO (SETIO) (90^o-100^oE, 10^oS-0^o), has been used in the literature to measure the surface variability internal to the Indian basin associated with the IOZM (Saji et al., 1999). Regression maps onto the IOZM index (right

panels in Fig. 4) show that in all fields the patterns induced by ENSO and by the IOZM are related, as the latter resemble the former with stronger amplitude. The time-series of Niño-3.4 and the IOZM are indeed correlated in the HadISST dataset with coefficient $r = 0.32$ if all months are considered, $r_{JJAS} = 0.57$ if the analysis is limited to monsoon season (see Fig. 9a). The high correlation, which increases to $r_{SON} = 0.62$ in boreal fall as noticed by Xie et al. (2002), the fact that several IOZM events are identified by significant SSTAs only on one side of the basin (Annamalai et al., 2003), and the absence of appreciable thermocline feedback in WTIO (Feng and Meyers, 2003) are the main ingredients for the interpretation of the IOZM as a forced mode of variability. On the other hand, both models and observations show that subsurface oceanic processes are important in SETIO during strong IOZM episodes, leading to the interpretation of the IOZM as a weak mode of variability, internal to the IO dynamics (Murtugudde et al., 2000; Rao et al., 2002; Gualdi et al., 2003; Saji and Yamagata, 2003; Bracco et al., 2005).

Undoubtedly, local and forced variability in the Indian Ocean is co-occurring, and a simple regression analysis (or Empirical Orthogonal Function analysis, as in Baquero-Bernal et al., 2002) may only portray a mixture of responses. The goal of this work is not, however, to distinguish between different contributions, but to see under which modelling conditions those inter-related responses can be properly simulated.

3.2 ENS1: The atmospheric teleconnections in the ICTP AGCM

In the AGCM-only ensemble, regression patterns with both Niño-3.4 (Fig. 5a) and the IOZM indices (Fig. 5b) display similar features. As in the case of other AGCMs, (see e.g. Wu and Kirtman 2004), the observed out-of-phase relationship between ENSO and Indian summer monsoon reverses, with a tendency towards increase rainfall over North India and the adjacent seas during the warm ENSO phase particularly during June and July. This is associated with a westerly wind anomaly blowing over the Arabian Sea during the monsoon season that brings moisture into the continent, opposite to the observations. In the AGCM,

warm ENSO events induce an increase in rainfall that, from the subtropical West Pacific, protrudes into the IO basin as a zonally elongated pattern, surrounded at higher and lower latitudes by regions with below-normal precipitation. As in the observations, drought conditions are particularly intense over Indonesia, and Sumatra. However, the model overestimates the cross-equatorial flow over the eastern IO, which brings moisture-rich air from the coast of Sumatra to the convergence areas over the Indochina peninsula and the West Pacific.

A better agreement between modelled and observed patterns can be found in the IOZM regressions, where the east-west difference in precipitation in the regions just south of the Equator is correctly simulated. In the northern subtropical regions, the simulated rainfall anomalies resemble the NCEP data more closely than the CMAP ones (as for the ENSO teleconnections). Note that, in both model and NCEP data, the signal is slightly negative over southern India contrary to CMAP and land station data (for land station data see Mason and Goddard, 2001).

The maps in Fig. 5 show regressions averaged over all the ensemble members. Although in individual years the internal variability of seasonal anomalies is rather large, 50-year regressions show similar tendencies among all members of the ensemble. Specifically, in association with El Niño conditions, no member displays the correct tendency of a wind anomaly opposing the summer monsoon circulation, nor a weakening of the ISMR.

3.3 ENS2: The thermodynamic mixed-layer and the role of the heat-fluxes

As pointed out by Lau and Nath (2000, 2003) and confirmed by the series of numerical experiments performed by Wu and Kirtman (2004), heat fluxes play a key role in the Indian Ocean. SST-forced AGCM simulations may fail in representing the air-sea coupling in the IO basin, and more generally in the tropical warm-pool region, since here SST anomalies originated by surface heat fluxes cannot be assumed as a driver of the atmospheric variability. In our second ensemble, a simple thermodynamics mixed-layer ocean model is implemented in the IO basin, from 35S to 30N and from the coast of Africa to 140E. The depth of

the mixed-layer is constant both in time and space and fixed to either 30 or 50 meters. In the following we will present results from the former ensemble. In summer and fall we did not find any significant dependency on the depth, but the observed SST warming anomaly associated to El Niño in spring (March-May) (e.g. Annamalai et al., 2003) is better simulated with a shallower mixed-layer, with a realistic pattern in the western and south parts of the basin and easterlies crossing the IO from Sumatra (see Fig. 6). Easterly winds, however, extend too far east to the coast of Africa when compared to NCEP reanalysis. This confirms the fundamental role played by the atmospheric teleconnections in spring.

Regressions with the Niño-3.4 index in JJAS are presented in Fig. 7. The northern and western part of the basin are characterized by a cold SST anomaly, a feature not present in the observations. This is due to a combination of reduced surface solar radiation and increased evaporation, which in turn results from the erroneous intensification of the near-surface westerly winds over the Arabian sea and India. However, the induced SST cooling tends to compensate the original errors noted in ENS1 over such regions, by reducing or suppressing convective activity (see the Appendix for a detailed description of the role played by evaporation and solar radiation in the various integrations). Our results broadly agree with the recent work by Shinoda et al. (2004), in which the authors analyzed the role of heat flux anomalies induced by variability in the Pacific over the Indian Ocean with a similar set-up, using the GFDL AGCM coupled to a more sophisticated mixed-layer model. In agreement with reanalysis data, they found that the net surface heat fluxes induced by El-Niño in the Western Indian Ocean and Arabian Sea during the monsoon season act to cool the sea surface temperatures. Ocean dynamics is therefore responsible for the warming of the Western IO (see Fig. 4a), as first suggested by Murtugudde and Busalacchi (1999).

The regression patterns for precipitation are closer to the observed signal. The negative anomaly extending westwards from Indonesia bends towards the Indian peninsula, reaching the subcontinent in 5 members out of 10 in JJAS and southern India in the ensemble mean. On the other hand, upwelling-favorable wind anomalies off Sumatra are absent during the monsoon season and the error

extents into the fall.

In this ensemble the definition of a IOZM index is mostly irrelevant. Here, the SST variability is only due to heat fluxes, while the zonal mode in the observations has a clear dynamical component, being characterized by upwelling and downwelling off Sumatra and Java, with surface and subsurface Kelvin and Rossby waves connecting SETIO and WTIO regions. Interestingly, the SST regression map with a non-realistic IOZM index, defined only on anomalies generated by heat fluxes, is associated to a La-Niña-like SST pattern in the Pacific (not shown). This suggests that heat-flux anomalies induced by atmospheric teleconnections cannot account for the positive correlation between the observed IOZM and ENSO indices.

3.4 ENS3: The OGCM in the Indian Ocean and role of IO dynamics

When a dynamical ocean model is coupled to the ICTP AGCM in the Indian basin, results change quite substantially. In ENS3 surface heat fluxes and SSTs are consistent, and the ocean can adjust locally to changes in the evaporation; in addition, upwelling/downwelling events induced by wind anomalies are represented.

As in the case of the models used by Wu and Kirtman in two separate studies (Wu and Kirtman, 2004, 2005), the observed inverse ISMR-ENSO relationship is properly simulated, as shown by the rainfall regression pattern in Fig. 8c. The anticorrelation between the El-Niño index and the Indian monsoon rainfall (defined as the rainfall anomaly averaged over land points in the region 70E-95E, 10N-30N) is -0.58 in the model ensemble and -0.6 in the gridded monthly precipitation data obtained from land stations (New et al., 1999). As already noted by Wu and Kirtman (2005), the improvement is related to a local negative feedback that leads to a weakening of the SST forced atmospheric response in the coupled simulations. Further discussion of this mechanism is presented in the Appendix.

On the other hand, the ENSO signature on the SST regression pattern (Fig. 8a) is much weaker than in the observations, in contrast with results for spring

(not shown), when more realistic amplitude and spatial patterns, closely resembling the ones in Fig. 6, are simulated. Similarly, ENSO-related wind anomalies are well modelled in March-May (not shown), whereas winds regressions during the monsoon season do not show the upwelling-driving signal off Java and Sumatra that characterizes the observations (Fig. 8c). In JJAS, the weak wind signal over SETIO in the ensemble regression pattern comes from the compensation of single-member patterns affected by substantial internal variability, and no individual member sustains the upwelling favorable winds modelled during spring through September.

As for the previous simulations, strong positive rainfall anomalies surround the Indochina peninsula during El Niño events. However, in the coupled runs the model error is reduced when compared to the SST-forced experiment because of the sea-surface cooling induced by variation in the heat fluxes (mainly, in surface solar radiation -see the Appendix) .

As already noticed in Bracco et al. (2005), in this ensemble the variability associated with the IOZM index results from an independent coupled mode, internal to the Indian Ocean dynamics, and displays a clear biennial cycle. The SST regression patterns onto the IOZM index (Fig. 8b) show a good resemblance to observations, at least in regions which are sufficiently distant from the boundaries of the ocean model domain. In ENS3 ENSO and the IOZM mode are independent from each other. The correlation between the Niño-3.4 and the IOZM indices is non significant, with a coefficient varying between -0.12 and 0.14 when all months are considered and analogous numbers for JJAS (see Fig. 9b). Air-sea feedbacks are crucial for the development of the IOZM, as the ocean responds locally to the winds, and remotely with the excitation of Rossby and Kelvin waves. Thermocline anomalies in SETIO during spring precondition the sign of the index for the following summer.

During positive IOZM events, anomalous winds strengthen the cyclonic circulation over southern India and upwell cold water off Sumatra. Wind anomalies south of 5^oS are weaker than in the NCEP-NCAR reanalysis, and so is the upwelling; however, the main features of the wind and rainfall regression over

the Indian ocean, shown in Fig. 8d, are reasonably well simulated. Consistent with the absence of significant SST anomalies in the Indonesian region (affected by the eastern boundary conditions of the ocean model), negative precipitation anomalies do not extend into Indonesia and are centered few degrees north of the observed signal.

The independence of ENSO and the IOZM in ENS3 makes the regression patterns associated with these modes more different from each other than their observational counterparts, shown earlier in Fig. 4. If the observed correlation between Niño and the IOZM indices is artificially imposed, most of the characteristics of the observed ENSO regressions can be recovered. In Fig. 10 we show the summer regression maps constructed as

$$< reg_{N3.4new} >=< reg_{N3.4j} * [(1-r^2_{obs})(1-r^2_{MODj})]^{1/2} + r_{obs} * reg_{IOZMj} >_{j=1,10} . \quad (2)$$

r_{obs} is the observed correlation coefficient between the IOZM and the Niño-3.4 time series in the HadISST dataset during JJAS, r_{MODj} the modelled one for each j-member of the ensemble, and $reg_{N3.4j}$ and reg_{IOZMj} j-member regressions. Patterns of SST, wind and rainfall anomalies improve significantly, despite the tendency for a northward displacement of the signal over the Maritime continent and excessive precipitations over South China sea and surrounding areas. Rainfall regression closely resembles the one obtained for the NCEP reanalysis (Fig. 4c). This result suggests that the model is able to simulate the observed patterns, but the mechanisms connecting the Pacific and the Indian basins are not (all) properly represented in the present configuration.

3.5 ENS4: The ICTP AGCM forced by ENS3 SSTs and the role of interactive coupling

In ENS4 we isolate the role of interactive versus "two-tier" coupling over the IO, by forcing the ICTP AGCM with the sea surface temperature of ENS3. As for the climatology, few significant differences are found in the variability patterns of the ensemble. All regressions resemble the ones obtained for ENS3, with a slightly stronger signal (see Fig. 11 for the regressions with the Niño-3.4 index to be compared with Fig. 8c). Winds and rainfall anomalies have the same sign

and location.

In most areas, evaporation anomalies have the same sign as SST anomalies during summer. In particular, during the warm ENSO phase, they are negative over the northern part of the Bay of Bengal, opposing the westward extension of the positive rainfall anomalies from Indochina and the South China Sea.

Our results differ slightly from the findings of Wu and Kirtman (2004) and Wang et al. (2005). In their simulations the interactive coupling appears to be a necessary condition for recovering the ENSO-ISMR inverse relationship. In our model, we need an interactive coupling to generate SST anomalies which are consistent with the heat-fluxes generated by the AGCM. Once the ACGM is forced by the SSTs generated by the coupled model the patterns associate with interannual variability are preserved in the ensemble average. This suggests that the hypothesis of Lau and Nath (2003) and Wang et al. (2005), i.e. that rainfall over South-east Asia is not a response to the SST variability but a cause of sea surface temperature anomalies is correct, but that different AGCMs are affected by the interactive coupling in different ways. In this work the suppression of the interactive coupling in ENS4 produces mainly an enhancement of the atmospheric response. Once the SSTs and the modelled heat fluxes are consistent the effect of the coupling is limited to a damping of the signal. In the experiments by Wu and Kirtman (2004) and Wang et al. (2005) the internal variability of the AGCM on sub-seasonal time-scales is such to impact the patterns of the interannual response in the absence of the ocean damping. Models resolution and complexity may play a key role. Notably, in the AGCM intercomparison analysis by Sperber and Palmer (1996), it was found that few AGCMs forced by observed SSTs were able to simulate the observed ENSO-ISMR teleconnection.

Our findings seem to indicate that the degree of internal variability in the AGCMs response is an important factor, which varies with horizontal and vertical resolution and with the convective closure schemes.

In interpreting the results from ENS4, it should be noticed that a faithful reproduction of 50-year long statistics does not imply that the predictability of interannual variations is the same in coupled and prescribed SST experiments. In

fact, the difference in the representation of air-sea interactions between coupled and forced runs is added to the effects of internal atmospheric variability. To assess the relative importance of these two factors, the ENS4 ensemble has been replicated using slightly different initial conditions for the model atmosphere. We shall refer to this additional ensemble as ENS4b (note that in ENS4, as well as in ENS4b, each member is forced with the SST of one single member of ENS3, which differ from other members over the Indian Ocean). Now the seasonal-mean anomalies from the 10 ENS4 runs (each including 50 years) can be used as predictors of the corresponding anomalies, i.e. associated with the same SST, in both ENS4b and ENS3. In the former case, the reproducibility is only affected by the internal atmospheric variability, while in the latter both internal variability and a different representation of air-sea interactions play a role.

Fig. 12 shows scatter diagrams of JJAS rainfall anomalies averaged over the area (75-85E, 10-25N), covering most the Indian peninsula; ENS4 anomalies (on the x-axis) are used as "predictors" of ENS4b anomalies (left panel) and ENS3 anomalies (right panel) for all the 500 simulated seasons (50 years times 10 IO-SST realizations). The correlation coefficients are 0.48 for the forced-vs-forced case, and 0.38 for the forced-vs-coupled case. As a reference, if the ENS3 rainfall anomalies were simply regressed against the Nino3.4 index (therefore with no information about IO SST), the (absolute) correlation would drop to 0.29.

In the hypothesis that the forced component of the modelled Indian-rainfall variability is given by the ensemble-mean of a large ensemble with the *same* SST, the correlation between anomalies from two individual experiments is equivalent to the fraction of variance explained by the forced component. Therefore, we can estimate that such a component accounts for 48% of the total variance in SST-forced run. On the other hand, if we had replicated ENS4 many times and computed the ensemble-mean of such realizations for each season and IO-SST, such a mean would only explain 30% ($= 0.38^2$ / 0.48) of the variance of the ENS3 Indian rainfall. We conclude that, in our experiments, the mismatch between air-sea coupling over the IO in forced and coupled runs reduces the fraction of "predictable" variance by almost a factor of 2. This result is obviously a model

estimate obtained with exactly the same AGCM in both configurations; as such, it gives an upper limit to the predictability obtainable with the so-called two-tier approach to climate predictions, where SSTs from coupled simulations are used to drive ensembles of AGCM runs with, for example, higher horizontal resolution.

3.6 ENS5: The role of oceanic teleconnections

In ENS5 the numerical integrations include an active ocean model also in the Pacific, with climatological SST imposed elsewhere. The variability of the Pacific and Indian Ocean are now connected also through the oceanic bridge, and strong IOZM events are often associated with ENSO episodes (see also Bracco et al., 2005). The correlations between the IOZM and ENSO indices are significant, with very similar coefficients in all members and in 50-years long sub-sampling of the 150-years time-series. When considering all months in the year, coefficients are 0.44, 0.46 and 0.43 for the three members respectively; in JJAS, the average correlation raises from 0.44 to 0.47, in close agreement with the observed value of 0.53 (see Fig. 9c).

The modelled IOZM index is of larger amplitude than the observed, as the SST anomalies in SETIO are often stronger than in the HadISST dataset. In the SETIO region the SSTs are influenced by a surface barrier layer (Sprintall et al. 1992), which cannot be properly simulated by the bulk mixed-layer representation in MICOM. Indeed, if an analogous index is constructed on the anomalies below the surface (for example using the variability of the 20^o isotherm -Z20-, a proxy for the thermocline depth, in SETIO and WTIO) the agreement between model and Simple Ocean Data Assimilation (SODA) reanalysis (Carton et al., 2000) is very good (Bracco et al., 2005). The ENSO seasonal cycle and its interannual variability is well represented in the model. El Niño episodes are, however, slightly stronger than observed in amplitude, and warm SST anomalies extend 5-10^o too far west in the Pacific compared to the observations (Fig. 13).

The role played by the ocean bridge in the ENSO-IOZM relation, and the influence exerted by ENSO on the ocean subsurface in SETIO has been recently investigated by Bracco et al. (2005) and Annamalai et al. (2005).

The presence of a realistic ocean teleconnection in ENS5 induces not only a realistic ENSO-IOZM correlation, but also regression patterns in better agreement with the observations. The variability associated with ENSO (left panels in Fig. 14) is now characterized by wind anomalies favoring upwelling in SETIO, starting in late spring and intensifying through summer and autumn. In JJAS strong positive rainfall anomalies are confined to the West Pacific and are probably associated to stronger than observed warming produced by the modelled El Niño in this region. The extension and amplitude of SST variability is in good agreement with HadISST data, except for the absence of warm SST anomalies below 25S. This problem is common to other coupled models (see for example Huang and Shukla, 2006), where the presence of a blending region and climatological SSTs at the southern boundary prevents a proper simulation of the atmospheric teleconnections between the Southern Indian Ocean and the Antarctic circumpolar regions (Lau and Nath, 2004).

Good agreement with the observations is also found in the case of the IOZM regression maps (Fig. 14, right panels). Anomalies over the Indian basin are well positioned and of the correct sign and strength. Excess rainfall during positive IOZM events extend to East Africa in the following season (October to December) (not shown), modulating the short rains (Black et al., 2003; Clark et al., 2003). The model however reproduces only partially the observed amplitude of the intensified local meridional circulation associated with IOZM events (Behera et al., 1999; Annamalai et al., 2003; Annamalai and Liu (2005)), which is slightly weaker than in the reanalysis along the western coast of the Indian subcontinent (compare Fig. 14d with Fig.4f). As a result the model does not fully reproduce the positive precipitation anomaly over India. The intensification of the monsoon circulation in the model is stronger if only July and August are considered, as in the observations. During those two months rainfall slightly increases over land.

As in the case of the ENSO regressions, warm SSTAs (and therefore deep convection) extend too far west in the Pacific, and model winds induce a convergence of moisture over the South China Sea. NCEP rainfall regressions contain a similar signal (Fig. 4d). The CMAP dataset, on the other hand, display an

extensive region of below-normal precipitation extending from SETIO into the West Pacific (Fig. 4f).

In ENS6 the SSTs of ENS5 are used to force the ICTP AGCM, and the regression patterns described above are recovered with a slightly more intense amplitude for both wind and precipitation (not shown). The out-of-phase relationship between ENSO and the ISMR is preserved also in ENS6. The conclusions derived for ENS4 are therefore confirmed also in presence of a realistic relation between ENSO and IOZM.

4 Discussion and conclusions

In this study, we have compared ensemble numerical simulations of the South Asian summer monsoon performed with a hierarchy of models, in which the interactions between the atmospheric and oceanic circulations in the tropical Indo-Pacific region are represented with increased degree of complexity. The main goal of this comparison is to identify the "ingredient", in terms of coupling strategy and spatial domain, that are needed to properly represent the relationship between SST anomalies (in both the Pacific and Indian Ocean) and anomalies in monsoon wind and rainfall patterns.

In the first ensemble, where AGCM simulations are forced by globally prescribed SST (ENS1), the absence of proper air-sea coupling leads to a clearly incorrect simulation of the ENSO-monsoon relationship. In the second ensemble, where a simple thermodynamic mixed-layer model is used in the tropical Indian Ocean (ENS2), feedbacks induced by heat fluxes partially correct the deficiencies of the SST-forced experiment, but still fail to produce the correct anomaly patterns as a response to ENSO anomalies prescribed in the tropical Pacific. The modelled rainfall response to ENSO becomes more realistic when the mixed layer model is replaced by a dynamical ocean model in the IO (ENS3). In ENS3, IO dynamics allows the development of internal variability associated with the Indian Ocean zonal mode (IOZM). However, with SST still prescribed in the Pacific, the Indian and Pacific basins are only connected through the atmospheric circulation, which prevents the development of the proper relationship between

SST variability in the two oceans. As a consequence, SST wind and rainfall anomalies simulated in ENS3 as responses to ENSO and the IOZM fail to reflect the observed correlation between the two phenomena. Only when the domain of the dynamical ocean model is extended to include the tropical Pacific (ENS5), the coupled model succeeds to simulate the correct ENSO-IOZM relationship, through a preconditioning of sub-surface waters in the south-eastern tropical IO. This link is reflected in the regression of monsoon wind and rainfall onto the corresponding SST indices, one notable effect being the partial compensation of opposite rainfall signals over the Indian subcontinent.

Our results on the importance of air-sea coupling for the proper simulation of interannual variability in the IO region are in agreement with a number of recent studies (e.g. Wu and Kirtman, 2004; Wang et al., 2005). However, we wish to stress that thermodynamic effects, as represented in a mixed-layer model, are not enough to recover the correct response to ENSO during the northern summer and fall. This has implications, for example, in the case of dynamical downscaling of seasonal predictions, where regional climate models may fail to represent the proper rainfall response if a simple thermodynamic mixed layer is used at the lower boundary. Furthermore, when the actual monsoon anomalies are determined by the interplay between ENSO and the IOZM (such as in summer 1997), the correct simulation of their correlation is essential to estimate the ENSO response in terms, for example, of anomalies in Indian rainfall. In this respect, our experiments highlight the importance of the sub-surface link between the Indian and Pacific oceans, which makes the "recipe" for the correct simulation of Asian monsoon variability increasingly complex. In addition to the seasonal prediction problem mentioned above, these results should be borne in mind when analysing the projections of future climate scenarios over the south Asian regions, particularly when they are originated from time-slice AGCM experiments when air-sea coupling is not properly represented.

On the other hand, regarding the usefulness of simulations with prescribed SST, the results of the ensemble in which SST from the IO dynamical model were prescribed to the AGCM (ENS4) are probably more positive than what reported

in recent literature (e.g. Wang et al. 2005), as ENS4 recovered the same ENSO-monsoon statistics displayed by ENS3. However, our results are obtained using exactly the same AGCM at the same resolution as in the coupled system, and therefore may not be relevant to the case of AGCM simulations forced by SST produced by different models at coarser resolution.

In summary, although our results confirm the importance of a coupled modelling strategy as the best (and probably the only appropriate) recipe for the simulation of the interannual and interdecadal variability of the Asian monsoon, it appears that the degree of realism obtainable with different modelling frameworks (e.g. two-tier seasonal predictions, regional model simulations, time-slice experiments) may be dependent on individual model characteristics, and in particular on the amount of internal, chaotic atmospheric variability affecting the simulated monsoon flow. The fact that many AGCMs tend to over-estimate such a component (e.g. Molteni et al. 1993) may itself be a result of the absence of air-sea feedbacks, but may also arise from modelling deficiencies which affect predictability estimates in a negative way. The ICTP AGCM, with its coarse resolution and parameterizations optimized for the simulation of climate variability, may provide different results from models mainly developed for weather forecasting. A proper analysis of the intraseasonal variability of the monsoon flow in the ICTP model will be the subject of future investigations.

Acknowledgments

The experiments described were performed as a contribution to the ENSEMBLES project funded by the European Commission's 6th Framework Programme, contract number GOCE-CT-2003-505539.

The authors wish to thank Ben Kirtman for useful discussions during the preparation of this manuscript, and Hari Annamalai and an anonymous referee for their valuable comments and suggestions that helped improving the manuscript.

5 Appendix

The goal of this appendix is to provide the reader with a quantitative assessment of the modelled surface fluxes.

A detailed analysis of the surface heat fluxes in the various ensembles and a complete understanding of the model response is beyond the goal of this work and will require further integrations and possibly more idealized set-ups. We think, however, that a presentation of the latent heat flux and of the surface solar radiation will allow for a better comparison between our integrations and results from recently published work.

In agreement with the findings of Wu and Kirtman (2004), ENS1, forced by observed SST, is characterized by evaporation anomalies that follow surface wind anomalies (Fig A1a) during ENSO events. In the warm phase, positive SST anomalies in the eastern IO are associated to anomalous winds favorable to the advection of moisture into the Indian subcontinent, absent in the reanalysis. Correspondingly a strong peak in evaporation is centered off the Somali coast. The surface solar radiation, on the other hand, is directly correlated with the precipitation pattern, erroneously strong over India.

In the coupled cases (ENS3 and ENS5), latent heat flux anomalies in the eastern part of the basin are negatively correlated with SST anomalies (panels (c) and (g)). Such a relations is preserved when the SSTs generated by the coupled model are used to force the ICTP AGCM (for ENS4 panels (e) and (f); ENS6 not shown). The signal, however, has a stronger amplitude, evident especially in the latent heat flux regression map. The comparison between panels (c) and (e) confirms the role played by the interactive ocean model, which damps part of atmospheric variability. Such a damping is found also in the analysis of integrations performed with other models. The ICTP AGCM, however, differs from other models (e.g. Wu and Kirtman, 2004; Wang et al., 2005) as it is able to preserve the main patterns of variability whenever is forced by SSTs previously created by the model heat fluxes.

From the analysis of the surface solar radiation variability, it appears that cooling anomalies associated with positive ENSO events over the Indochina penin-

sula in ENS3 are related to a decrease of surface solar radiation, associated with the excess of precipitation produced by the model in this region. The confinement of such anomaly over the West Pacific in ENS5, in better agreement with the observations, supports the conclusion of Wu and Kirtman (2004), who advocated the need of a fully coupled model over the West Pacific to properly simulate the latitudinal extension of convective precipitation in the Indo-Pacific basin.

References

Allan RJ, Chambers D, Drosdowsky W, Hendon H, Latif M, Nicholls N, Smith I, Stone R, Tourre Y (2001) Is there an Indian Ocean dipole, and is it independent of the El Niño Southern Oscillations? CLIVAR Exchanges: 6(3) 18–22

Annamalai H, Liu P (2005) Response of the Asian summer monsoon to changes in El Niño properties. Quart J Roy Meteor Soc 131: 805–831

Annamalai H, Murtugudde R (2004) Role of the Indian Ocean in regional climate variability. Earth's Climate: The ocean-atmosphere interaction. AGU Geoph Monograph Ser 47

Annamalai H, Murtugudde R, Potemra J, Xie SP, Liu P, Wang B (2003) Coupled dynamics over the Indian Ocean: spring initiation of the zonal mode. Deep-Sea Res II 50: 2305–2330

Annamalai H, Potemra J, Murtugudde R, McCreary JP (2005) Effect of preconditioning on the extreme climate events in the tropical Indian Ocean. J Clim 18: 3450–3469

Arpe K, Dumenil L, Giorgetta MA (1998) Variability of the Indian monsoon in the ECHAM3 model: Sensitivity to sea surface temperature, soil moisture, and the stratospheric quasi-biennial oscillation. J Clim 11: 1837–1858

Bamzai AS, Marx L (2000) COLA AGCM simulation of the effect of anomalous spring snow over Eurasia on the Indian summer monsoon. Quart J Roy Meteor Soc 126: 2575–2584

Baquero-Bernal A, Latif M, Legutke M (2002) On dipole-like variability of sea surface temperature in the tropical Indian Ocean. J Clim 15: 1358-1368

Behera SK, Krishnan R, Yamagata T (1999) Unusual ocean-atmosphere conditions in the tropical Indian Ocean during 1994. Geoph Res Let 26, 3001–3004, 10.10129/1999GL010434

Black E, Slingo J, Sperber KR (2003) An observational study of the relationship between excessively strong short rains in coastal East Africa and Indian Ocean SST. Mon Wea Rev 131: 74–94

Bleck R, Rooth C, Hu D, Smith LT (1992) Salinity-driven thermocline transients in a wind- and thermocline-forced isopycnic coordinate model of the North Atlantic. J Phys Ocean 22: 1486–1505

Bracco A, Kucharski F, Rameshan K, Molteni F (2004) Internal variability, external forcing and climate trends in multi-decadal AGCM ensembles. Clim Dyn 23: 659–678

Bracco A, Kucharski F, Molteni F, Hazeleger W, Severijns C (2005) Internal and forced modes of variability in the Indian Ocean. Geoph Res Let 32: doi 10.1029/2005GL023154

Bourke W (1974) A multilevel spectral model. I: Formulation and hemispheric integrations. Mon Weat Rev 102:687–701

Carton JA, Chepurin G, Cao X, Giese B (2000) A simple ocean data assimilation analysis of the global upper ocean 1950-95. Part I: methodology. J Phys Ocean 30: 294-309

Clark C, Webster PJ, Cole JE (2003) Interdecadal variability of the relationship between the Indian Ocean Zonal Mode and East African coastal rainfall anomalies. J Clim 16: 548–554

Corti S, Molteni F, Palmer TN (1999) Signature of recent climate change in frequencies of natural atmospheric circulation regimes. Nature 398: 799-802

Douville H, Royer J-F (1996) Sensitivity of the Asian summer monsoon to an anomalous Eurasian snow cover within the Météo France GCM. Clim Dyn 12: 449-466

Feng M, Meyers G (2003) Interannual variability in the tropical Indian Ocean. A two-year time-scale of Indian Ocean Dipole. Deep-Sea Res II 50: 2263–2284

Ferranti L, Molteni F (1999) Ensemble simulations of Eurasian snow-depth anomalies and their influence on the Asian summer monsoon. Quart J Roy Meteor Soc 125: 2597-2610

Fisher AS, Terray P, Guilyardi E, Gualdi S, Delecluse P (2005) Two Independent Triggers for the Indian Ocean Dipole/Zonal Mode in a Coupled GCM. J Clim, 18: 3428–3449

Gualdi S, Guilyardi E, Navarra A, Masina S, Delecluse P (2003) The interannual variability in the tropical Indian Ocean as simulated by a CGCM. Clim Dyn 20: 567–582

Hackert EC, Hastenrath S (1986) Mechanisms of Java rainfall anomalies. Mon Weat Rev 114: 745–757

Hastenrath S (2002) Dipoles, temperature gradients, and tropical climate anomalies. Bull Am Meteorol Soc 83: 735-740

Hastenrath S, Nicklis A, Greischar L (1993) Atmospheric-hydrospheric mechanisms of climate anomalies in the western equatorial Indian Ocean. J Geoph Res 98: 20219–20235

Hazeleger W, Molteni F, Severijns C, Haarsma R, Bracco A, Kucharski F (2003) SPEEDO: A flexible coupled model for climate studies. CLIVAR Exchanges 28

Held IM, Suarez MJ (1994) A proposal for the intercomparison of the dynamical cores of atmospheric general circulation models. Bull Am Meteorol Soc 75: 1825–1830

Huang B, Shukla J (2006) On the mechanisms of the interannual variability in the Tropical Indian Ocean. Part I: The role of remote forcing from the Tropical Pacific. J Clim. In Press

Ju J and Slingo JM (1995) The Asian summer monsoon and ENSO. Quart J Roy Meteor Soc 121: 1133-1168

Kalnay E, Kanamitsu M, Kistler R, Collins W, Deaven D, Gandin L, Iredell M, Saha S, White G, Woollen J, Zhu Y, Chelliah M, Ebisuzaki W, Higgins W, Janowiak J, Mo C, Ropelewski C, Wang J, Leetmaa A, Reynolds R, Jenne R, Joseph D (1996) The NCEP/NCAR 40-Year Reanalysis Project. Bull Amer Meteor Soc 77: 437-471

Kinter JL, Miyakoda K, Yang S (2002) Recent changes in the connection from the Asian monsoon to ENSO. J Clim 15: 1203–1214

Krishna-Kumar K, Rajagopalan B, Cane MA (1999) On the weakening relationship between the Indian monsoon and ENSO. Science 284: 2156–2159

Krishnamurthy V, Kirtman BP (2003) Variability of the Indian Ocean: Relation to monsoon and ENSO. Quart J Roy Meteor Soc 129: 1623–1646

Kucharski F, Molteni F, Bracco A (2006) Decadal interactions between the western tropical Pacific and the North Atlantic Oscillation. Clim Dyn 26: 79-91 doi: 10.1007/s00382-005-0085-5

Iizuka S, Matsuura T, Yamagata T (2000) The Indian Ocean SST dipole simulated in a coupled general circulation model. Geoph Res Let 27: 3369–3372

Latif M, Barnett TP (1995) Interaction in the tropical Oceans. J Clim 8: 952–964

Lau NC, Nath MJ (2000) Impact of ENSO on the variability of the Asian-Australian monsoons as simulated in GCM experiments. J Clim 13: 4287–4309

Lau NC, Nath MJ (2003) Atmosphere-ocean variations in the Indo-Pacific sector during ENSO episodes. (2003) J Clim 16: 3–20

Lau NC, Nath MJ (2004) Coupled GCM simulation of the atmosphere-ocean variability associated with zonally asymmetric SST changes in the tropical Indian Ocean. J Clim 17: 245–265

Levitus S, Conkright ME, Boyer TP, Burgett R (1994) World Ocean Atlas 1994 [CD-ROM data sets], NOAA, Silver Spring, MD.

Li T and Zhang Y (2002) Processes that determine the quasi-biennial and lower frequency variability of the South Asian monsoon. J Met Soc Japan 80: 1449–1163

Mason SJ, Goddard L (2001) Probabilistic precipitation anomalies associated with ENSO. Bull Am Meteor Soc 82: 619–638

McPhaden MJ (1999) Genesis and evolution of the 1997-1998 El Niño. Science 283: 950–954

Molteni F (2003) Atmospheric simulations using a GCM with simplified physical parameterizations. I. Model climatology and variability in multi-decadal experiments. Clim Dyn 20: 175–191

Molteni F, Corti S, Ferranti L, Slingo JM (2003) Predictability experiments for the Asian summer monsoon: Impact of SST anomalies on interannual and intraseasonal variability. J Clim 16: 4001–4021

Murtugudde R, Busalacchi AJ (1999) Interannual variability of the dynamics and thermodynamics of the tropical Indian Ocean. J Clim 12: 2300–2326

Murtugudde R, McCreary JP, Busalacchi AJ (2000) Oceanic processes associated with anomalous events in the Indian Ocean with relevance to 1997-1998. J Geoph Res 105: 3295–3306

New M, Hulme M, Jones PD (1999) Representing twentieth century space-time climate variability. Part I: Development of a 1961-90 mean monthly terrestrial climatology. J Clim 12: 829–856

Rao AS, Behera SK, Masumoto Y, Yamagata T (2002) Interannual variability in the subsurface tropical Indian Ocean. Deep-Sea Res II 49: 1549–1572

Rasmusson EM, Carpenter TH (1983) The relationship between the eastern Pacific sea surface temperature and rainfall over India and Sri Lanka. Mon Wea Rev 111: 517–528

Rayner NA, Parker DE, Horton EB, Folland CK, Alexander LV, Rowell DP, Kent EC, Kaplan A (2003) Global analyses of SST, sea ice, and night marine air temperature since the late nineteenth century. J Geoph Res 108 (D14), 4407, doi:10.1029/2002JD002670

Reverdin G, Cadet LD, Gutzler D (1986) Interannual displacements of convection and surface circulation over the equatorial Indian Ocean. Quart J Roy Meteor Soc 112: 43-67

Rodwell MJ, Rowell DP, Folland CK (1999) Oceanic forcing of the wintertime North Atlantic Oscillation and European climate. Nature 398: 320–323

Ropelewski CF, Halpert MS (1987) Global and regional scale precipitation patterns associated with the El Niño/Southern Oscillation. Mon Wea Rev 115: 1606–1626

Saji NH, Goswami BN, Vinayachandran PN, Yamagata T (1999) A dipole mode in the tropical Indian Ocean. Nature 401: 360–363

Saji NH, Yamagata T (2003) Structure of SST and surface wind variability during Indian Ocean Dipole Mode events: COADS observations. J Clim 16: 2735–2751

Schott F, McCreary JP (2001) The monsoon circulation of the Indian Ocean. Progr Oceanogr 51: 1–123

Shukla J (1975) Effect of Arabian sea-surface temperature anomaly on Indian summer monsoon: A numerical experiment with the GFDL model. J Atmos Sci 32: 503-511

Shukla J (1987) Interannual variability of monsoon. In *Monsoons, Fein and Stephens, Eds. Wiley*: 399–464

Shukla J, Paolino DA (1983) The Southern Oscillation and long range forecasting of the summer monsoon rainfall over India. Mon Weat Rev 111: 1830–1837.

Slingo JM, Annamalai H (2000) 1997: The El Niño of the century and the response of the Indian summer monsoon. Mon Wea Rev 128: 1778-1797

Sperber KR, Palmer TN (1996) Interannual tropical rainfall variability in general circulation model simulations associated with the atmospheric model intercomparison project. J Clim 9: 2727–2750

Sprintall J, Chong J, Syamusdin F, Morawitz W, Hautala S, Bray N, Wijffels S (1999) Dynamics of the South Java current in the Indo-Australian basin. Geoph Res Lett 26: 2493–2496

Susanto RD, Gordon AL, Zheng Q (2001) Upwelling along the coast of Java and Sumatra and its relation to ENSO. Geoph Res Let 28(8): 1599–1602

Tourre YM, White WB (1995) ENSO signals in global upper ocean temperature. J Phys Ocean 25: 1317–1332

Turner AG, Inness PM, Slingo JM (2005) The role of the basic state in the ENSO-monsoon relationship and implications for predictability Quart J Roy Meteor Soc 131: 781-804

Venzke S, Latif M, Villwock A (2000) The coupled GCM ECHO-2. Part II: Indian Ocean response to ENSO. J Clim 13: 1371–1383

Wang B, Ding Q, Fu X, Kang IS, Jin K, Shukla J, Doblas-Reyes F (2005) Fundamental challenge in simulation and prediction of summer monsoon rainfall. Geoph Res Let 32: doi 10.1029/2005GL022734

Wang BR, Wu R, Li T (2003) Atmosphere-warm ocean interaction and its impacts on the Asian-Australian monsoon variation. J Clim 16: 1195–1211

Webster PJ, Magana VO, Palmer TN, Shukla J, Tomas RA, Yanai M, Yasunari T (1998) Monsoons: Processes, predictability, and prospects for prediction. J Geophys Res 103: 14452–14510

Webster PJ, Moore AM, Loschnigg JP, Leben RR (1999) Coupled ocean-atmosphere dynamics in the Indian Ocean during 1997-98. Nature 401: 356-360

Webster PJ, Yang S (1992) Monsoon and ENSO: Selectively interactive systems. Quart J Roy Meteor Soc 118: 877–926

Wu R, Kirtman BP (2004) Impacts of the Indian Ocean on the Indian summer monsoon-ENSO relationship. J Clim 17: 3037–3054

Wu R, Kirtman BP (2005) Roles of Indian and Pacific ocean air-sea coupling in tropical atmospheric variability. Clim Dyn 25: 155–170

Xie P, Arkin PA (1997) Global precipitation: a 17-year monthly analysis based on gauge observations, satellite estimates and numerical model outputs. Bull Am Meteorol Soc 78: 2539–2558

Xie SP, Annamalai H, Schott FA, McCreary JP (2002) Structure and mechanisms of south Indian Ocean climate variability. J Clim 15: 867–878

Yamagata T, Behera S, Rao SA, Guan Z, Ashok K, Saji NH (2003) Comments on "Dipoles, temperature gradient and tropical climate anomalies". Bull Amer Meteor Soc 84: 1418–1422

Zhang Y, Wallace JM, Battisti DS (1997) ENSO-like Interdecadal Variability: 1900-93. J Clim 10: 1004-1020

Experiment	Ensemble	Description	To investigate
ENS1	10 members	**ICTP AGCM** forced by globally prescribed HadISSTs from 1950 to 1999	The Indo-Pacific atmospheric teleconnection in the ICTP-AGCM
ENS2	10 members	Prescribed HadISSTs from 1950 to1999 except in the tropical Indian Ocean (33S-30N, 20E-143E) where a **thermodynamic mixed layer** is implemented	The role of heat fluxes in the ENSO-ISMR relationship
ENS3	10 members	Prescribed HadISSTs from 1950 to1999 except in the region (32S-30N, 20E-140E) where **MICOM** is coupled to the ICTP AGCM	The role of the Indian Ocean dynamics in the ENSO-ISMR relation in the absence of an oceanic bridge with the Pacific
ENS4/ ENS4b	10 +10 members	Globally prescribed HadISSTs in the period 1950-1999 except in the tropical Indian Ocean where SSTs from ENS3 are used to force the AGCM	Interactive versus "two-tier" coupling over the Indian Ocean. The role of internal variability.
ENS5	3 members 150 years long	Climatological SSTs except in the tropical Indo-Pacific ocean (32S-30N) where MICOM is coupled to the ICTP AGCM	The role of the oceanic bridge between the Indian and the Pacific ocean in the ENSO-IOZM relation
ENS6	3 members 150 years long	Climatological SSTs except in the tropical Indo-Pacific ocean (32S-30N) where SSTs from ENS5 are used to force the AGCM	Interactive versus "two-tier" coupling in the tropical Indo-Pacific

Table 1: List and description of the experiments discussed in the paper.

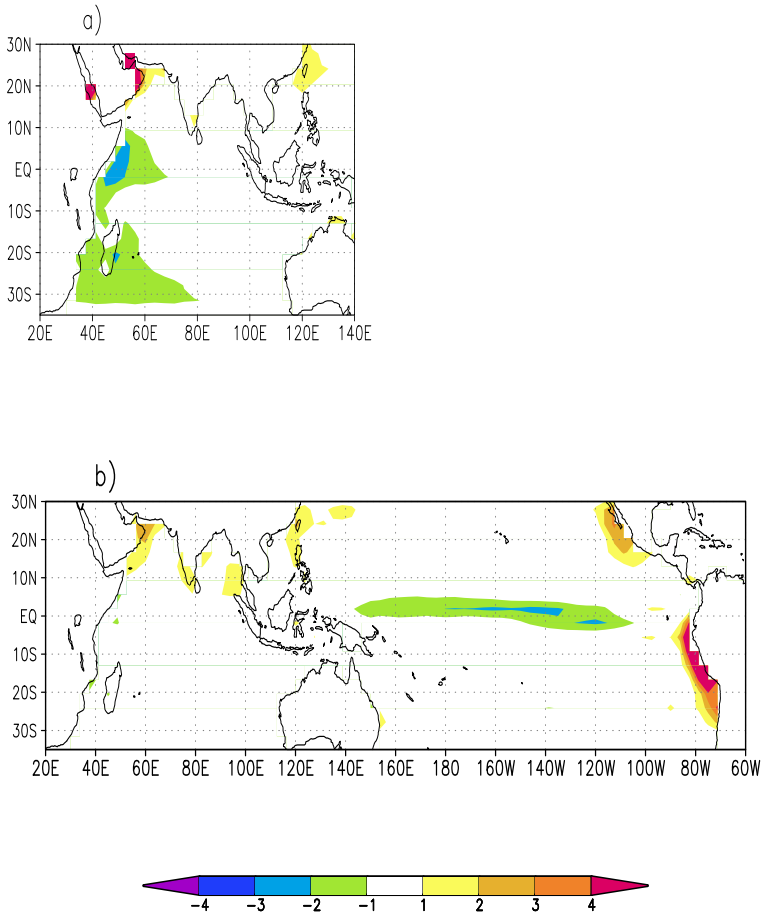

Figure 1: Difference between observed and model SST climatology during JJAS in a) ENS3 and b) ENS5.

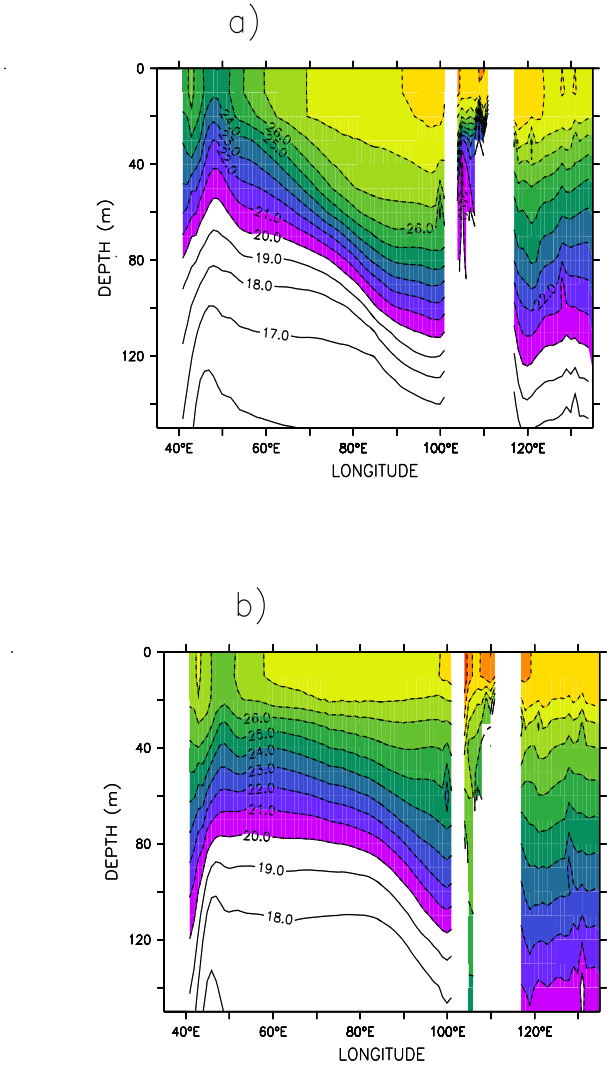

Figure 2: Annual mean vertical profile of temperature in the first 150m of the water column in the Indian basin at the equator (averaged over 2S-2N) in a) ENS3 and b) ENS5. The region above the 20^o isotherm, a proxy for the thermocline depth, is shown in color.

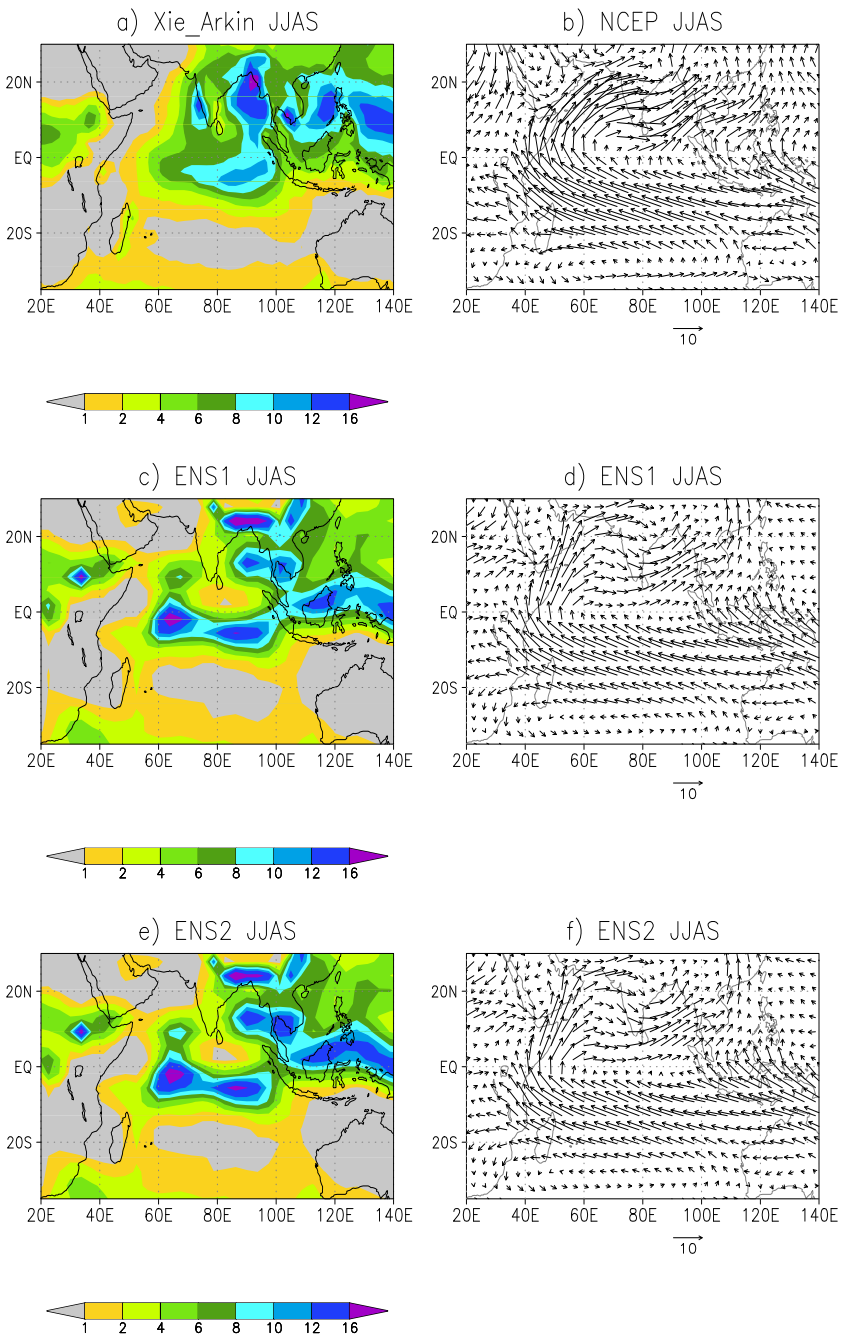

Figure 3: a) Observed climatology of JJAS rainfall over the period 1979-2002 (CMAP data) and b) of 925hPa winds over the period 1950-1999 (NCEP data). Below the modelled climatology of boreal summer precipitation and 925hPa winds for ENS1 (panel c-d), ENS2 (e-f), ENS3 (g-h) and ENS4 (i-j) respectively.

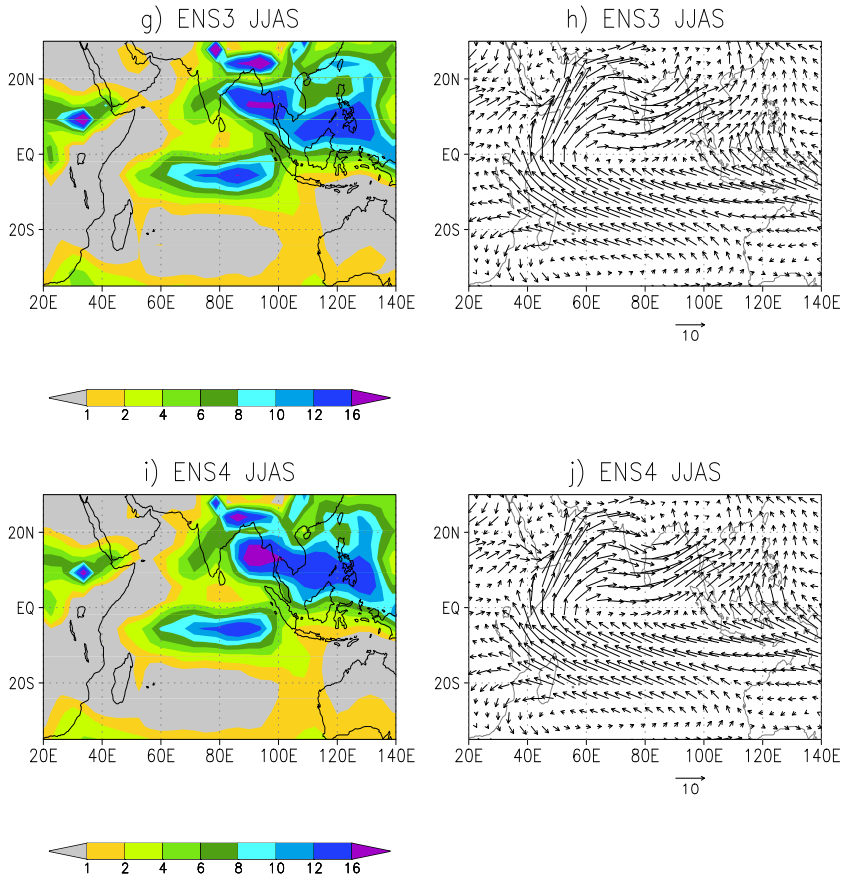

Figure 3 continued

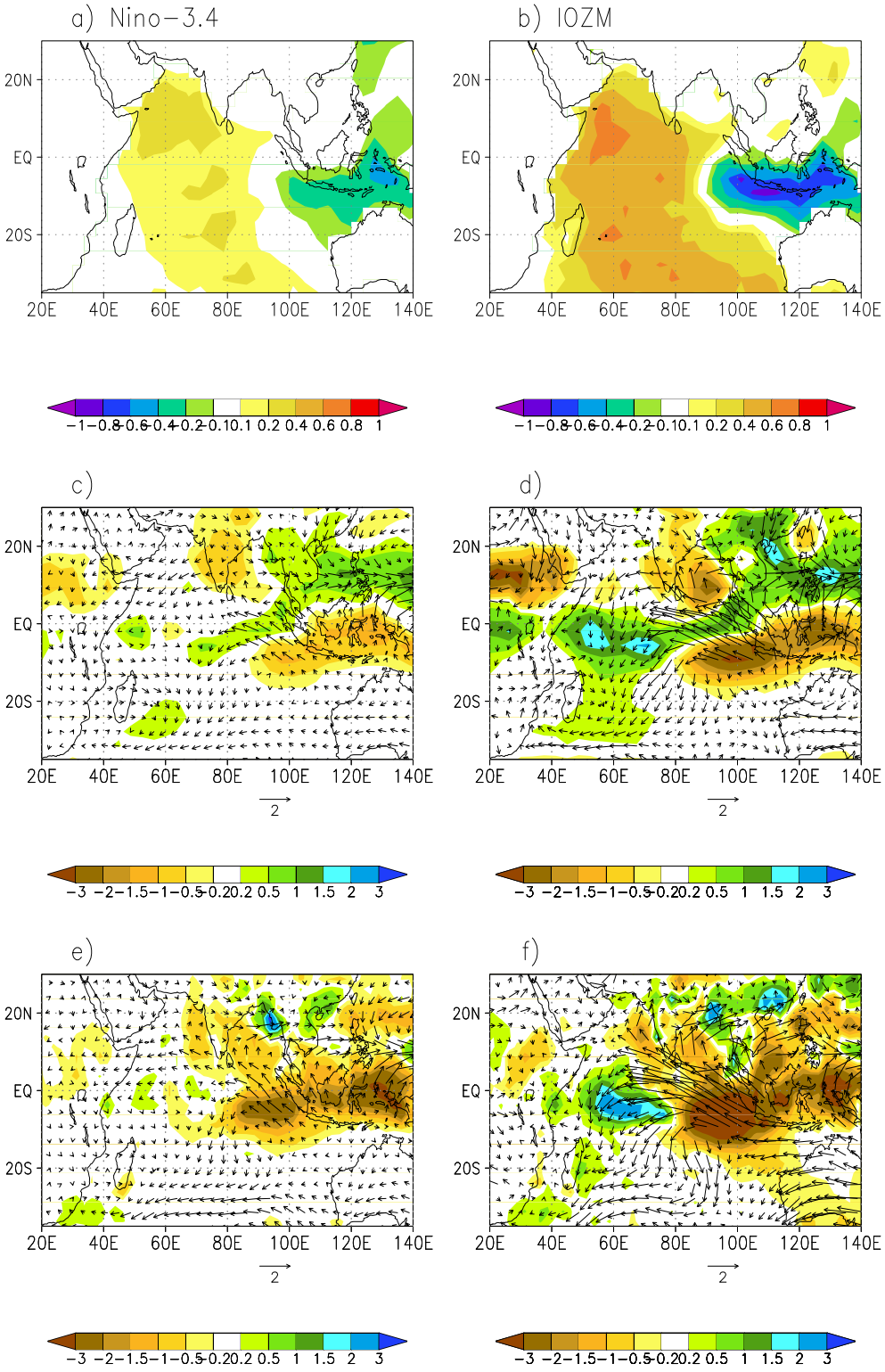

Figure 4: Distribution of the regression coefficients vs the Nino-3.4 index (left panels) and vs the IOZM index (right panels) of a)-b) the SST field using HadISST data (period 1950-1999), c)-d) precipitation and 925 hPa winds using NCEP reanalysis for the second half of the 20th century, and e)-f) CMAP data 925Pa NCEP winds over the period 1979-2002, during JJAS.

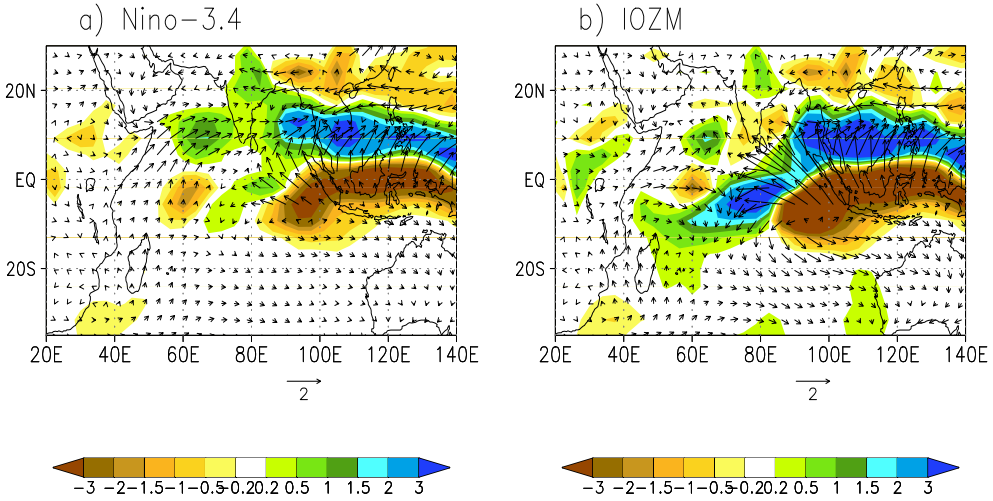

Figure 5: ENS1. Ensemble average distribution of the regression coefficients of the modelled rainfall and 925hPa wind fields vs Nino-3.4 (a) and vs the IOZM (b) indices in JJAS over the period 1950-1999.

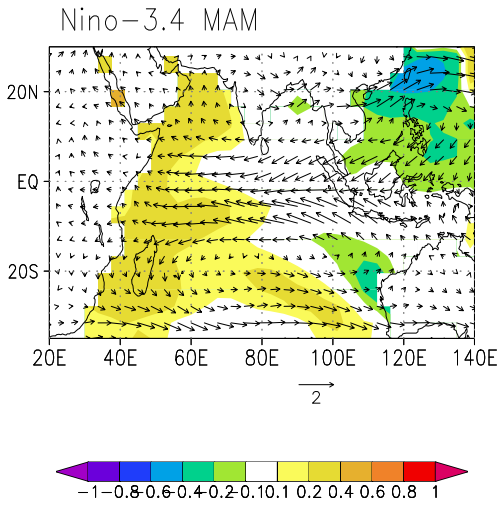

Figure 6: ENS2. Ensemble average distribution of the regression coefficients vs Nino-3.4 index of the modelled SST field and 925 hPa winds during spring (MAM).

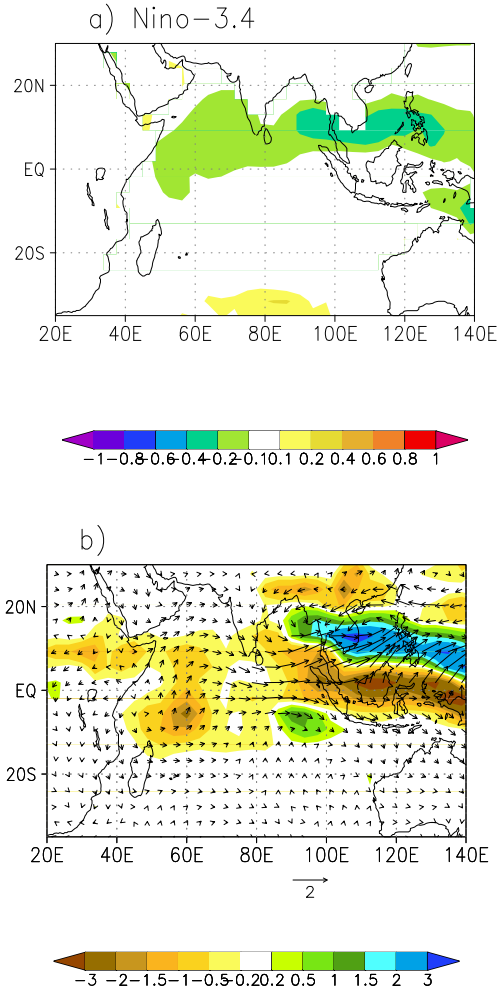

Figure 7: ENS2. Ensemble average distribution of the regression coefficients vs Nino-3.4 index of the modelled SST field (a) and precipitation and 925 hPa winds (b), during JJAS.

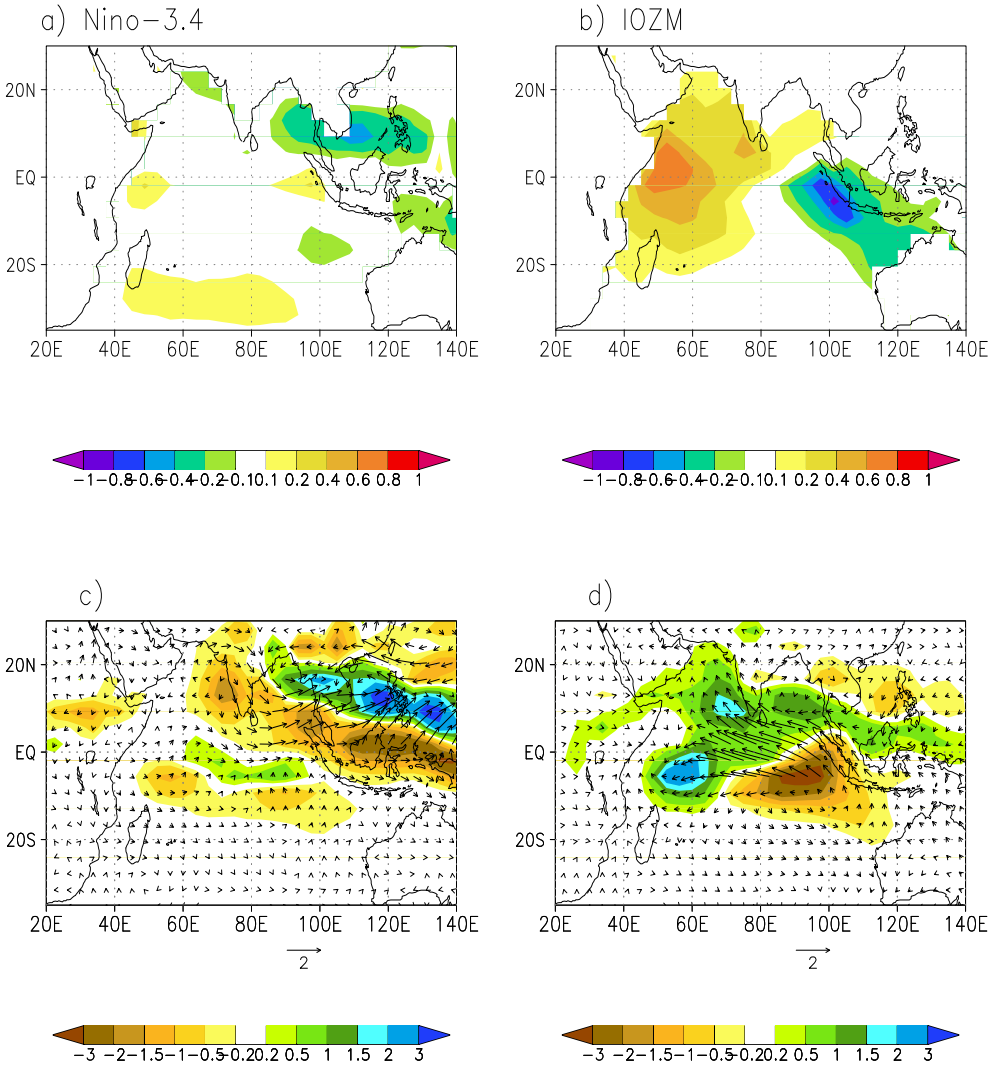

Figure 8: ENS3. Ensemble average distribution of the regression coefficients vs Nino-3.4 (left panels) and IOZM (right panels) indices of the modelled SST field (a-b) and of precipitation and 925 hPa winds (c-d) respectively, during JJAS.

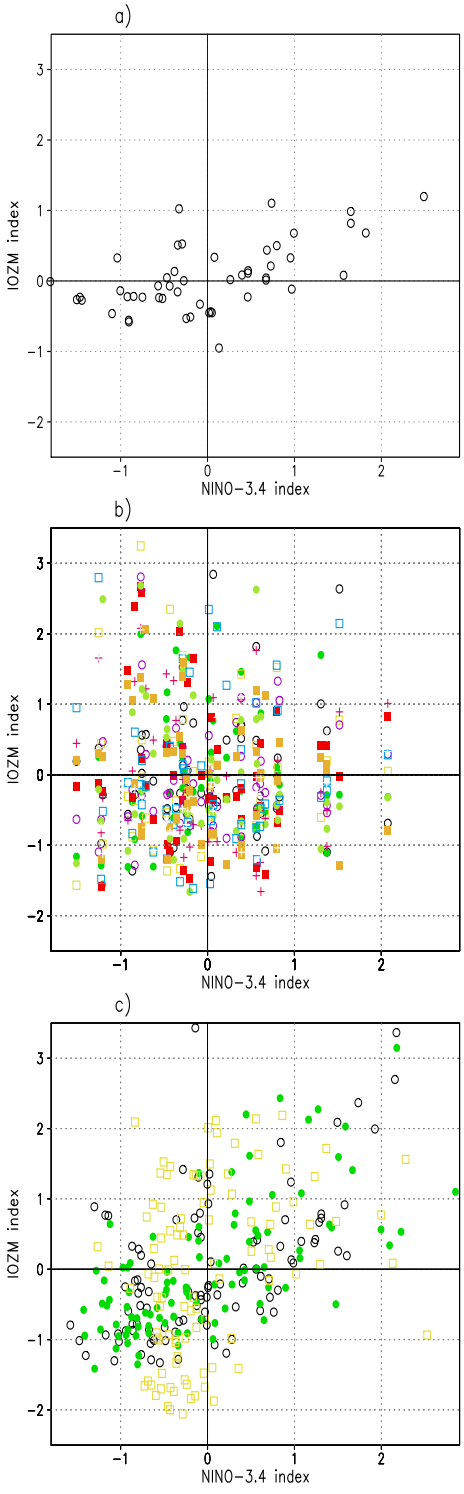

Figure 9: Scatter plot of the IOZM vs the Nino-3.4 index for each individual JJAS season in the HadISST dataset (a), ENS3 (b), ENS5 (c).

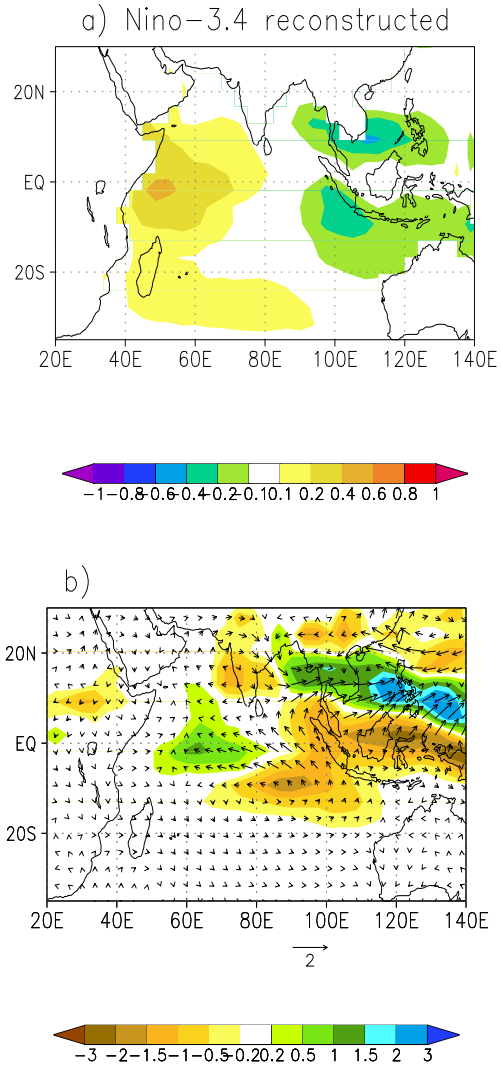

Figure 10: ENS3. Ensemble average distribution of the regression coefficients of JJAS SST anomalies (a) and rainfall and 925hPa winds (b) vs the Nino-3.4 index constructed imposing the observed correlation between Nino-3.4 and IOZM indices. See text for details.

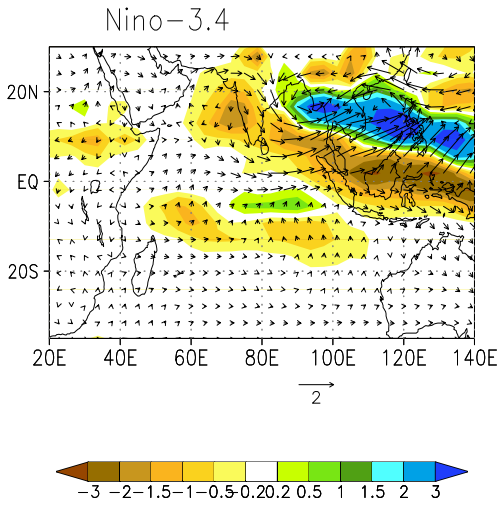

Figure 11: ENS4. Ensemble average distribution of the regression coefficients vs Nino-3.4 index of the modelled precipitation and 925 hPa winds during JJAS.

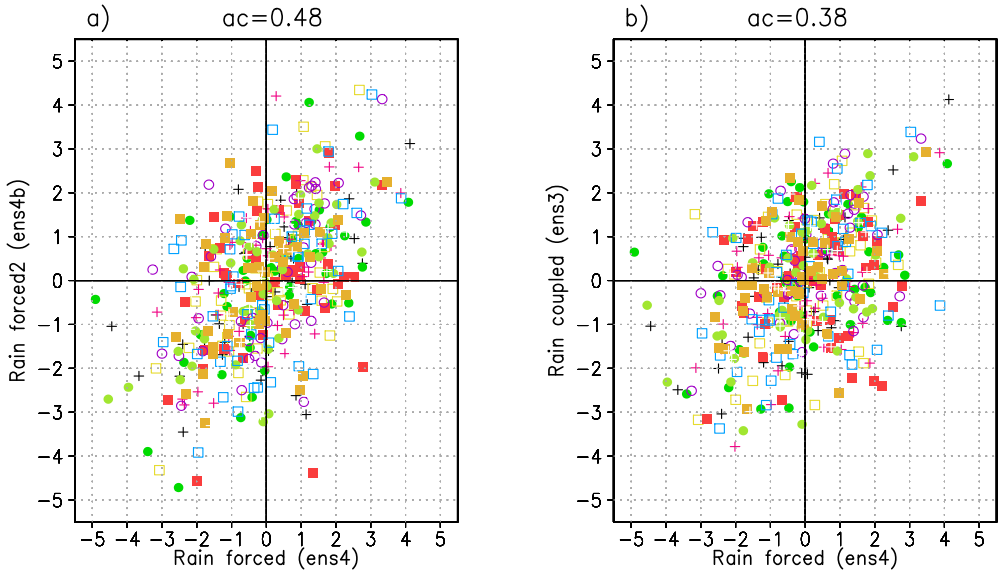

Figure 12: Scatter diagrams of JJAS rainfall anomalies averaged over the Indian peninsula (area 75-85E, 10-25N) in ENS4 vs ENS4b (a) and ENS4 vs ENS3 (b) for the 50 simulated seasons for each of the 10 realizations (different colors).

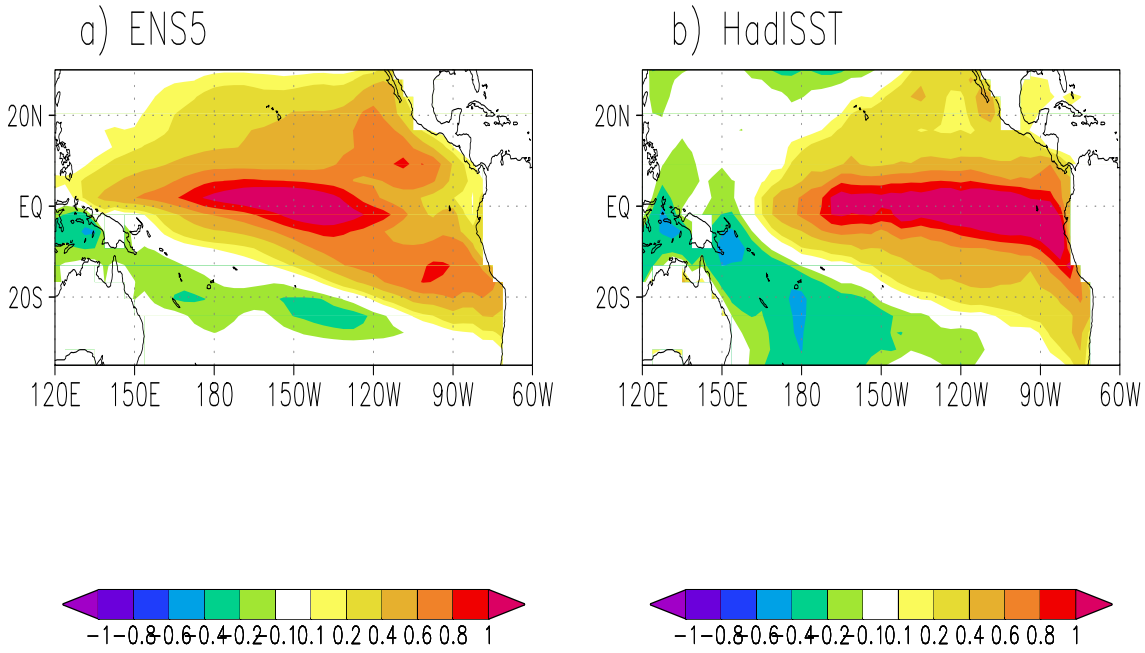

Figure 13: Distribution of the regression coefficients vs the model Nino-3.4 index in JJAS over the Pacific Ocean for (a) ENS5 (ensemble average) modelled SST and (b) the HadISST dataset.

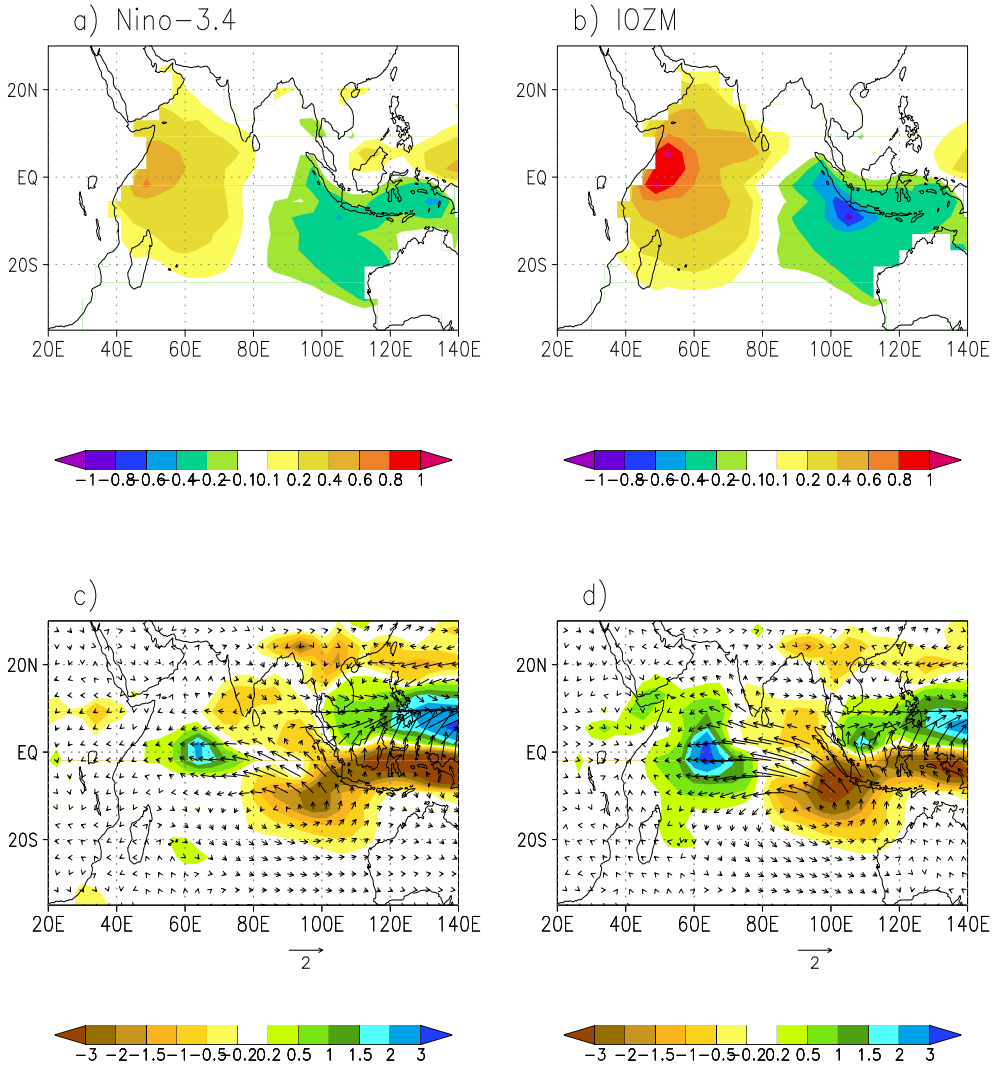

Figure 14: ENS5. Ensemble average distribution of the regression coefficients vs Nino-3.4 (left panels) and IOZM (right panels) indices of the modelled SST field (a-b) and of precipitation and 925 hPa winds (c-d) during JJAS.

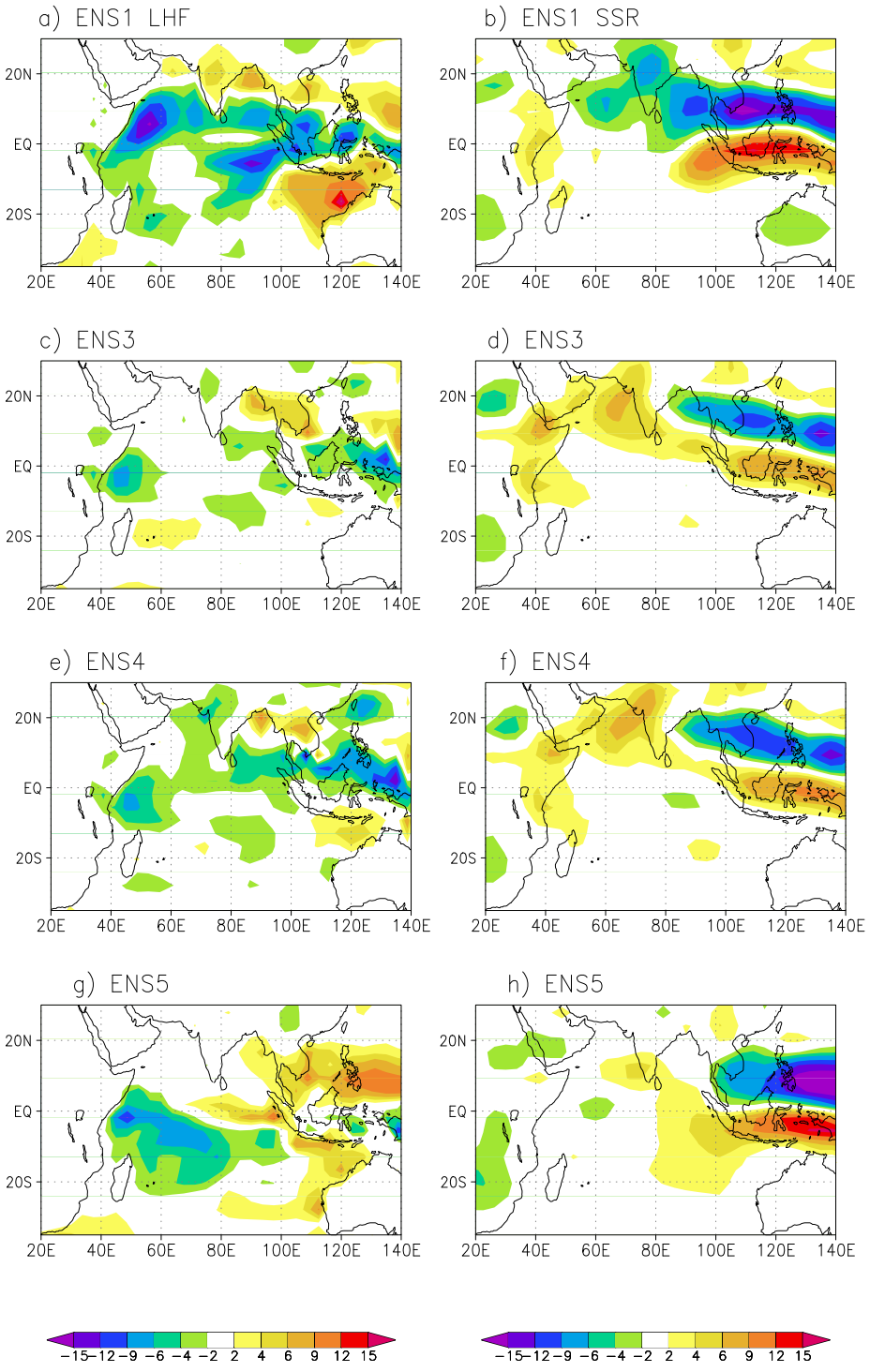

Figure A1: Ensemble average distribution of the regression coefficients of the modelled latent heat flux (left column) and of surface solar radiation (on the right) vs the model Nino-3.4 index for a)-b) ENS1, c)-d ENS3, e)-f) ENS4, and g)-h) ENS5 (in W/m^{-2}).